Applied Catalysis B: Environmental 241 (2019) 95–103

Contents lists available at ScienceDirect

Applied Catalysis B: Environmental

journal homepage: www.elsevier.com/locate/apcatb

Novel and multifunctional inorganic mixing salt-templated 2D ultrathin Fe/Co-N/S-carbon nanosheets as effectively bifunctional electrocatalysts for Zn-air batteries

Chuanhua Li[a], Hanxing Liu[a,b,*], Zhiyong Yu[a,*]

[a] State Key Laboratory of Advanced Technology for Materials Synthesis and Processing, Wuhan University of Technology, Wuhan 430070, PR China
[b] International School of Materials Science and Engineering, Wuhan University of Technology, Wuhan 430070, PR China

ARTICLE INFO

Keywords:
Salt-template
Porous carbon nanosheets
Fe/Co-N/S-Cs
Electrocatalysts
Zn-air batteries

ABSTRACT

2D bimetallic and bi-nonmetallic codoping porous carbon nanosheets with more accessible surface area and active sites are especially potential electrocatalyst for oxygen reduction and oxygen evolution reaction (ORR and OER) of Zn-air batteries but the synthesis of this material has been rarely reported owing to excessively harsh requirements. Here, bimetallic (Fe/Co) and bi-nonmetallic (N/S) codoping porous carbon nanosheets (Fe/Co-N/S-Cs) with uniform and ultrathin thickness of about 4.63 nm were first synthesized by a novel and multifunctional inorganic mixing salt-template ($FeCl_3$ and $CoSO_4$). Fe/Co-N/S-Cs exhibit ultrahigh specific surface area (SSA: 1589 $m^2 g^{-1}$), total pore volume (TPV: 0.92 $cm^3 g^{-1}$), homogeneous distribution of heteroatom dopants, as well as an appropriate amount of carbon defects. Fe/Co-N/S-Cs show high half-wave potential ($E_{1/2}$ = 0.832 V) for ORR and extremely low overpotential of 285 mV at 10 mA cm^{-2} for OER, exceeding most reported electrocatalysts. Furthermore, assembled Zn-air batteries employing Fe/Co-N/S-Cs as cathode catalyst exhibit high power density (102.63 mW cm^{-2}) and excellent stability. This investigation sheds light on syntheses of superior but cheap electrocatalysts for developing next energy-related storage technology.

1. Introduction

In order to search for the economical, environmental and renewable energy technology, rechargeable metal-air batteries have got greatly growing interest on account of safety, environmental benignity, especially high theoretical energy density [1,2]. The one of most challenges of metal-air batteries is seriously high overpotential caused by sluggish kinetics of oxygen reduction and oxygen evolution reaction (ORR and OER) [3]. Consequently, seeking high-effective bifunctional electrocatalysts is extremely crucial to greatly prompt electrochemical processes of ORR and OER. At present, the high-active ORR catalysts are Pt-based materials and its derivatives, whereas the most prominent OER catalysts are Ir/Ru-based materials and their derivatives [4,5]. Nevertheless, the large-scale commercial implementation of noble metal based catalysts is hampered by high price, exiguity and poor stability. Therefore, it is especially vital to develop high-catalytic but less-expensive bifunctional catalysts [6,7].

Recently, transition metal nitrogen carbon (M-N-C, such as, Fe-N-C and Co-N-C) catalyst, which exhibits excellent electrocatalytic activity, has drawn intensive attention owing to its bifunctional electrocatalytic activity [8,9]. As a result, bimetallic doped (mainly enhancing OER activity of carbonous materials) M-N-C catalysts (such as Fe/Co-N-C [10,11]) with coexistence of abundant active Fe-Nx/Co-Nx sites and bi-nonmetallic doping (mainly improving ORR activity of carbonous materials) M-N-C catalysts (for example, Fe-N/S-C [12], Co-Nx/By-C [13]) with effectively modulated electronic properties of carbonous materials by bi-nonmetallic heteroatom dopants are extensively investigated to improve electrocatalytic performance. Many experimental results demonstrate that S heteroatom introduced into N-doping carbon can effectively promote catalytic activity on account of forming thiophene sulfur in carbon matrix [12,14,15]. In addition, theoretical calculation indicates that intrinsic carbon defects, which play an extremely important role on electrochemical processes of ORR, can be tailored by doping S atom to optimize catalytic performance [16]. Similarly, bimetallic doping carbon (for instance, Fe/Co-N-C [17–19]) also displays impressive bifunctional catalytic activity because of bimetallic heteroatom dopants effectively improving OER activity. However, the electrocatalytic activity of these modified M-N-C catalysts still exists in

* Corresponding authors at: State Key Laboratory of Advanced Technology for Materials Synthesis and Processing, Wuhan University of Technology, Wuhan 430070, PR China.
E-mail addresses: lhxhp@whut.edu.cn (H. Liu), yuzhiyong@whut.edu.cn (Z. Yu).

https://doi.org/10.1016/j.apcatb.2018.09.024
Received 11 July 2018; Received in revised form 3 September 2018; Accepted 8 September 2018
Available online 09 September 2018
0926-3373/

many shortcomings (such as, complex synthetic route, non-ideal electrocatalytic activity, low stability, etc.) for large-scale commercial implementation. In view of these reports, bimetallic (Fe/Co) and bi-nonmetallic (N/S) codoping carbonous materials should be particularly promising and high-active bifunctional catalysts. Unfortunately, this material (such as, Fe/Co-N/S-C) has been rarely reported because of excessively complex and control-difficult synthetic route.

The inorganic molten salt-template route was put forward by Antonietti [20] to obtaining facile, environmentally-friendly and scalable synthesis route of porous carbon. In this method, the mixtures of inorganic salt and carbon-containing precursor are firstly heated, then removing inorganic salt-template by aqueous washing. The nanostructures (such as SSA, TPV and morphology) of as-synthesized porous carbon largely depend on inorganic salts and carbon-containing precursors. Thence, researchers mainly focus on the effects of various inorganic salts (such as, LiCl, KCl,NaCl, $ZnCl_2$ and their mixed molten salts) and carbon-containing precursors on nanostructures of porous carbon [21–24]. In recent studies, this method is also employed to obtain tailor-made N-doped or S-doped porous carbon. Until recently, the investigations about using inorganic molten salt-template method to prepare bimetallic and bi-nonmetallic codoping carbonous catalysts are rarely reported. Furthermore, among the various porous carbon materials, 2D layered carbon materials exhibiting superior electrical charge transfer pathways [25–27] are especially remarkable succedaneum for precious metal catalyst because of high electrochemically accessible surface area and active sites which can prompt electrochemical reaction [15].

In view of previous studies and challenges, it is urgently needed to design convenient and control-easy fabrication procedure to achieve 2D layered Fe/Co-N/S-doped hierarchical porous carbon catalyst for effectively improving electrocatalytic performance. Based on these excessively harsh requirements, a novel and multifunctional inorganic salt mixing system ($FeCl_3$ and $CoSO_4$) is ingeniously designed to synthesize 2D layered Fe/Co-N/S-doped hierarchical porous carbon. The $FeCl_3{\cdot}6H_2O$ with 2D layered crystal structure [28] is mainly served as 2D layered inorganic molten salt-template to form layered porous carbon when the mixtures of $FeCl_3{\cdot}6H_2O$ and dopamine hydrochloride (DA) acted as carbon and nitrogen precursor are treated at high temperature. Meanwhile, $FeCl_3$ can also supply Fe doping and act as porogen to form hierarchical porous structure and DA provides N doping in carbon matrix during heat treatment. More importantly, $CoSO_4$ is firstly added to mixtures of $FeCl_3{\cdot}6H_2O$ and dopamine hydrochloride to offer Co and S heteroatom doping. Consequently, the novel and multifunctional inorganic salt mixture ($FeCl_3$ and $CoSO_4$) effectively breaks the barrier to derive 2D layered Fe/Co-N/S-doped hierarchical porous carbon.

Herein, the as-synthesized 2D ultrathin Fe/Co-N/S-doped hierarchical porous carbon nanosheets (Fe/Co-N/S-Cs) fabricated by mixing molten salt template ($FeCl_3$ and $CoSO_4$) exhibit ultrathin thickness (about 4.63 nm), ultrahigh SSA (1589 $m^2\,g^{-1}$) and TPV (0.92 $cm^3\,g^{-1}$). Impressively, the $CoSO_4$ molten salt forming novel inorganic salt mixing system with $FeCl_3$ not only increases SSA and TPV observably, but also improves N content (pyridinic N and graphitic N) and carbon defects owing to doping S atom. Consequently, the 2D ultrathin Fe/Co-N/S-Cs applied as electrocatalysts display effectively bifunctional performance for ORR and OER in alkaline solution, which are superior to state-of-the-art counterparts. In addition, Zn-air batteries employing Fe/Co-N/S-Cs as cathode catalysts exhibit high power density and excellent stability. The novel inorganic salt mixing template offers facile, environmental-friendly and scalable preparation route to rationally design practical and high-active 2D heteroatom-doped hierarchical porous carbon nanosheets, which sheds light on fabrication of superior but cheap electrocatalysts for developing next energy-related storage technology.

2. Experimental

2.1. Materials

$FeCl_3{\cdot}6H_2O$ (AR, 99%), $CoCl_2{\cdot}6H_2O$ (AR, 99%), CH_3OH (AR, 99.5%) and H_2SO_4 (AR, 98%) were provide by Sinopharm Chemical Reagent Co. Ltd. Dopamine hydrochloride (98%) and $CoSO_4{\cdot}7H_2O$ (AR, 99%) were provide by Sigma-Aldrich.

2.2. Synthesis of samples

Fe/Co and N/S codoping hierarchical porous carbon nanosheets (Fe/Co-N/S-Cs): The mixture powder of $FeCl_3{\cdot}6H_2O$, Dopamine hydrochloride (DA) and $CoSO_4{\cdot}7H_2O$ with molar ratio of 1:7:1 was ground until uniform mixing and immediately transferred into tube furnace. Then, the mixtures of dopamine and mixed salts were heated at 700 °C with heating rate of 5 °C/min under Ar environment for 120 min. The collected powder after cooling down to normal atmospheric temperature was washed with hot sulphuric acid (0.5 M) and deionized water to remove non-active substance and residual salts. Subsequently, final product of Fe/Co and N/S codoping hierarchical porous carbon nanosheets was dried at 80 ℃ overnight. As a comparison, Fe/Co and N codoping hierarchical porous carbon nanosheets (Fe/Co-N-Cs) were synthesized via similar approach except for molten salt template using $FeCl_3{\cdot}6H_2O$ and $CoCl_2{\cdot}6H_2O$. Simultaneously, Fe/N codoping porous carbon nanosheets (Fe-N-Cs) were also prepared by similar method except for molten salt template only using $FeCl_3{\cdot}6H_2O$.

2.3. Material characterization

Scanning electron microscopy (SEM) measurements were performed on JEM-7500F. Transmission electron microscopy (TEM) and high angle annular dark-field scanning transmission electron microscopy (HAADF-STEM) measurements were carried out on Talos F200S. X-ray photoelectron spectroscopy (XPS) was tested by ESCALAB 250Xi. N_2 adsorption-desorption isotherms were measured by Micromeritics ASAP 2020 instrument. LabRam HR Evolution serves as Raman measurements. D8 Advance acts as X-ray diffraction (XRD) measurements. Scanning probe microscope tests were recorded by Nanoscope IV.

2.4. Electrochemical measurements

The rotating disk electrode (RDE) measures were first performed to evaluate electrocatalytic performance of as-synthesized samples. The three-electrode measurement system consists of platinum wire electrode, Ag/AgCl electrode and glassy carbon substrate with geometric surface area of 0.07065 cm^2, acting as counter, reference and working electrode, respectively. The suspension including 0.8 mL of deionized water, 0.2 mL of isopropanol, 0.04 mL of 5 wt% Nafion solution and 5 mg catalysts was sonicated for about 0.5 h to form homogeneous catalyst ink. The polished glass carbon substrate as working electrode covered by 5 μL of catalyst ink was naturally dried for about 0.5 h to prepare homogeneous catalytic layer. The resultant electrochemical measurements were carry out on a potentiostat (CHI660B) at constant temperature of 25 °C. The cyclic voltammetry (CV) was first tested in N_2- and O_2-saturated potassium hydroxide aqueous solution (0.1 M) at 50 mV s^{-1}. The linear scanning voltammetry (LSV) at 10 mV s^{-1} was utilized to measure ORR polarization curves and OER polarization curves (at a rotating rate of 1600 rpm) in O_2-saturated solution. The rotating ring-disk electrode (RRDE) measurements were carried out to calculate H_2O_2 yield and electron transfer number (n) for ORR process. The electrochemical impedance spectroscopy (EIS) was measured in a frequency range of 1.0–1000 kHz with the amplitude of 5 mV.

Rechargeable zinc-air batteries were measured on self-made electrochemical cells. This cell mainly consists of zinc foil as negative electrode, Celgard 2332 as separator, carbon paper loaded by catalysts

(1.0 mg cm^{-2}) as positive electrode and 6.0 M KOH aqueous solution with 0.2 M $ZnAc_2$ as electrolyte. The charge-discharge measurements of zinc-air batteries were performed on the battery cycling system (LANHE-CT2001A).

3. Results and discussion

3.1. Preparation and structural characterization of catalysts

The inorganic salt-template ($FeCl_3$) combined with dopamine hydrochloride (DA) as nitrogen-containing carbon precursor was utilized to synthesize 2D heteroatom-doped hierarchical porous carbon nanosheets. $FeCl_3{\cdot}6H_2O$ with 2D layered crystal structure [28] could coordinate with dopamine (DA) to form the Fe-DA organic-inorganic coordination compound (in Fig. S1) under grinding at room temperature, because of Fe^{3+} with oxidizability and hydroxyl of DA with reducibility [29]. Subsequently, the layered porous carbon nanosheets were derived by thermal treatment of Fe-DA coordination compound under Ar atmosphere. Then, the produced metal nanoparticles during carbonization process and residual salt templates were eventually removed with repeated washing by sulphuric acid (0.5 M) solution and deionized water. The as-synthesized Fe-N-Cs show uniform nanosheets by SEM image (in Fig. 1a). As shown in Fig. 1d, the TEM image of Fe-N-Cs reveals that the ultrathin carbon nanosheet structures are formed by the pyrolysis of Fe-DA coordination compound and metal nanoparticles are not traced after acid washing. The purpose of adding $CoCl_2$ is to mainly achieve Co atom doping for effectively improving OER activity of Fe-N-Cs. Similarly, the Fe/Co-N-Cs also show similar morphology (in Fig. 1b) to Fe-N-Cs with addition of $CoCl_2$ and the ultrathin carbon nanosheet structures without tracing metal nanoparticles are also confirmed by the TEM image (in Fig. S2). In order to further enhance ORR activity of Fe/Co-N-Cs, $CoSO_4$ is added to form inorganic salt-template mixtures ($FeCl_3$ and $CoSO_4$) for sulfur doping compared to Fe/Co-N-Cs. Importantly, the carbon nanosheet morphology does not still change with addition of $CoSO_4$ (Fig. 1c). The TEM image (in Fig. 1e) confirms that Fe/Co-N/S-Cs possess ultrathin layered structures with several nanoparticles dispersed in carbon nanosheets, which is different from Fe-N-Cs and Fe/Co-N-Cs. Therefore, HRTEM image (in Fig. 1f) of Fe/Co-N/S-Cs ascertains that lattice fringes with interlayer distance of 0.2995 nm assigns to the (311) plane of Co_8FeS_8 nanocrystal with space group of $Fm\bar{3}m$, which is fully consist with XRD analysis (in Fig. S3). HAADF-STEM was further carried out to investigate element distribution. Fig. 2 verified that the N, S, Co and Fe dopants homogeneously distribute in porous carbon nanosheets for providing accessible catalytic sites. The strong Fe and Co element signals simultaneously appear in the area of nanoparticles due to the form of Co_8FeS_8, which has been confirmed by HRTEM image of Fe/Co-N/S-Cs (Fig. 1e) and XRD analysis (in Fig. S3). Recent studies have showed that Co_8FeS_8 exhibits excellent electrocatalytic performance for ORR and OER [30–32]. The schematic illustration of derived Fe/Co-N/S-Cs is shown in Scheme 1.

The XPS techniques were further performed to reveal the chemical composition and content of each element. The survey spectra disclose the presence of C, N, O, Fe and Co in Fe/Co-N-Cs and C, N, O, S, Fe and Co in Fe/Co-N/S-Cs, indicating that designed heteroatoms have been successfully doped into the carbon skeleton. From atomic percentages of the elements shown in Table S1, a significant change mainly takes place in total C and N contents. The total concentration of C element drops from 88.54% to 84.62% while total concentration of N element prominently increases from 5.09% to 8.09% for Fe/Co-N-Cs and Fe/Co-N/S-Cs. In general, the relatively high concentration of N element can be beneficial to electrochemical reaction of ORR [33,34]. The N1s region spectra of Fe/Co-N-Cs (Fe/Co-N/S-Cs) are deconvolved into four subpeaks at 398.38 eV (398.33 eV), 399.71 eV (399.70 eV), 400.97 eV (400.92) and 404.50 eV (404.62), respectively, attributable to pyridinic N, pyrrolic N and/or metal-bonded N, graphitic N and oxidized N in Fig. 3a and b [35,36]. From the relative content of different nitrogen types (in Table S2), pyridinic N and graphitic N are dominated, which are mainly beneficial for ORR catalysis [37]. Moreover, the relative content of pyridinic N in Fe/Co-N/S-Cs evidently increases and relative content of graphitic N slightly decreases in comparison with these in Fe/Co-N-Cs. In consideration of total concentration of N, the relative content of pyridinic N and graphitic N in Fe/Co-N/S-Cs is higher than that in Fe/Co-N-Cs. Simultaneously, the N1s XPS spectra of Fe-N-Cs is provided in Fig. S4. The N element concentration of Fe-N-Cs (5.77 At. %) is also lower than that of Fe/Co-N/S-Cs (8.09 At.%). The Fe 2p and Co 2p region spectra of Fe/Co-N/S-Cs are shown in Fig. S5, indicating that Fe-Nx and Co-Nx are formed via Fe/Co coordinating with N [10,11,38]. The deconvolution of the S 2p spectrum yielded three subpeaks at 163.83 eV for thiophene-sulfur (S $2p_{3/2}$), 165.02 eV for thiophene-sulfur (S $2p_{1/2}$) and 168.10 eV for oxidized sulfur (-C-SO_X-C-

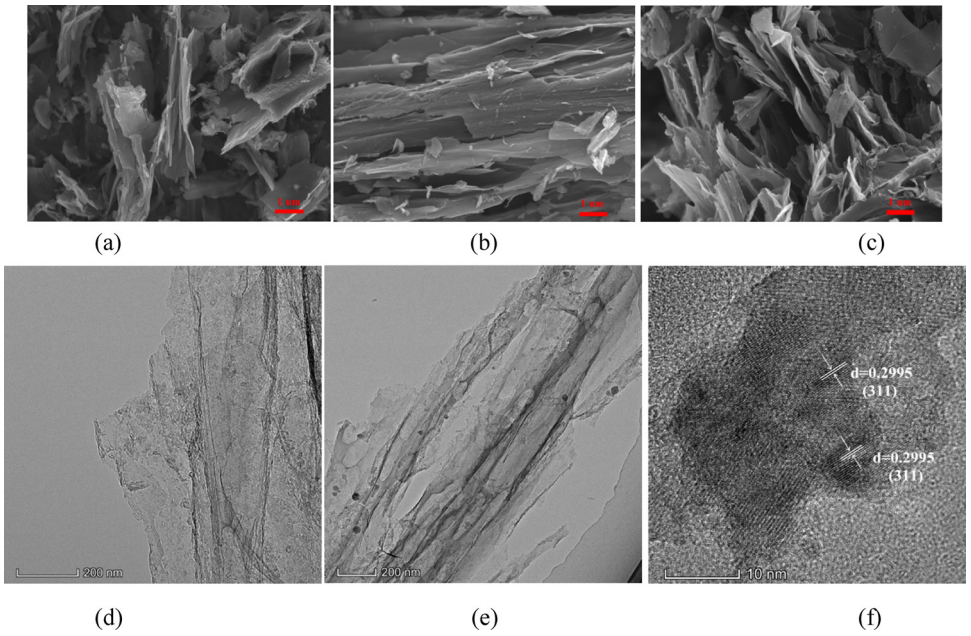

Fig. 1. SEM image of Fe-N-Cs (a), Fe/Co-N-Cs (b) and Fe/Co-N/S-Cs (c); TEM image of Fe-N-Cs (d) and Fe/Co-N/S-Cs (e); HRTEM image of Fe/Co-N/S-Cs (f).

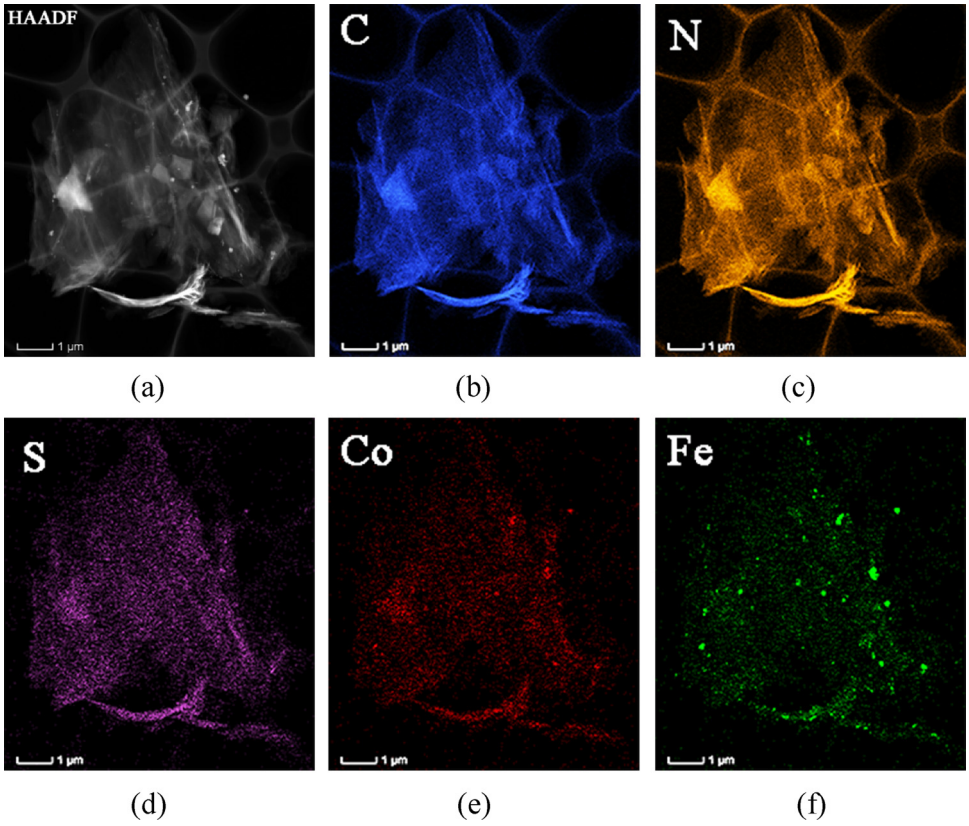

Fig. 2. HAADF-STEM image and the corresponding element mapping mages of C, N, S, Co and Fe.

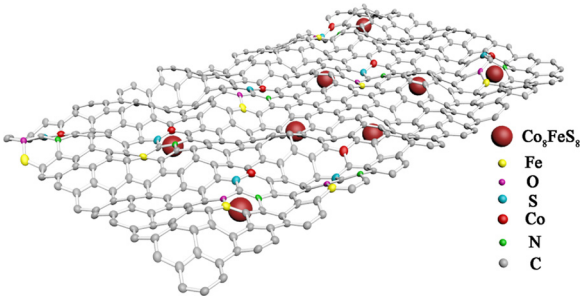

Scheme 1. Schematic illustration of as-synthesized Fe/Co-N/S-Cs.

), respectively [39,40], demonstating that sulfur was incorporated into carbon molecular skeletons by addition of $CoSO_4$ molten salt. In addition, Co_8FeS_8 nanoparticles with low contentare encapsulated by carbon nanosheets (confirmed by TEM image) and XPS techniques mainly study surface chemical composition so the XPS peak of Co_8FeS_8 does not appear. Based on DFT calculations by reported literature [41], the thiophene-sulfur atom can effectively boost catalytic performance for ORR because of mismatch between the outermost orbitals of the carbon atoms and neighboring thiophene sulfur atoms. As a result, the XPS analysis verifies that adding $CoSO_4$ molten salt not only successfully incorporates Co and S atoms into carbon molecular skeletons, but also effectively increases the nitrogen (especially pyridinic N) content.

The N_2-sorption measurements were further performed to investigate the porous characteristics of as-synthesized 2D ultrathin carbon nanosheets. As show in Fig. 4a, the SSA of Fe-N-Cs, Fe/Co-N-Cs and Fe/Co-N/S-Cs determined by BET method is 1235, 1624 and 1589 $m^2 g^{-1}$, respectively, and the isotherms show that carbon nanosheets with coexistence of micropores and mesopores mainly possess micropores. In addition, the TPV of Fe-N-Cs, Fe/Co-N-Cs and Fe/Co-N/S-Cs is 0.70, 0.94 and 0.92 $cm^3 g^{-1}$, respectively. In short, the addition of $CoCl_2$ or $CoSO_4$ forming mixed molten salt can observably increase the SSA and TPV of carbon nanosheets. The summary of SSA and TPV of currently reported M-N-C catalysts is displayed in Table S3, indicating

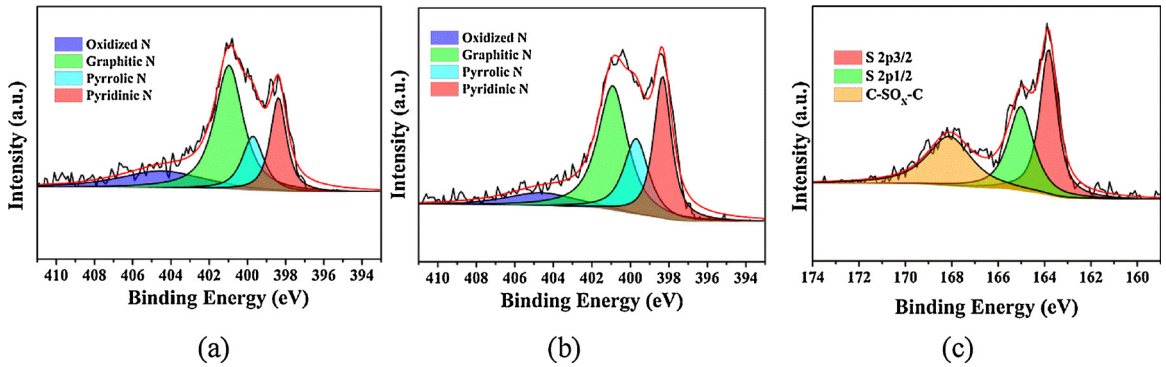

Fig. 3. N1s XPS spectra of Fe/Co-N-Cs (a) and Fe/Co-N/S-Cs (b); S 2p XPS spectra of Fe/Co-N/S-Cs (c).

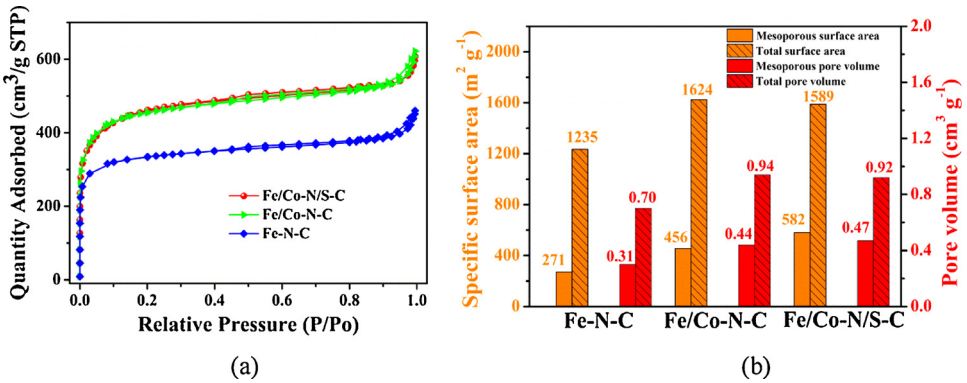

Fig. 4. (a) The N_2-sorption isotherms and (b) SSA and TPV of Fe-N-Cs, Fe/Co-N-Cs and Fe/Co-N/S-Cs.

that Fe/Co-N/S-Cs show higher SSA and TPV than most of the M-N-C catalysts reported in current literatures. For analyzing the carbon nanosheets porosity with addition of $CoCl_2$ or $CoSO_4$ in great detail, the mesoporous surface area (MSA) and mesoporous pore volume (MPV) of three samples are calculated by t-plot and the results are shown in Fig. 4b. The higher MSA and MPV formed during the pyrolysis of DA with molten salt template have a positive impact on the electrochemical reaction of ORR and OER [42]. The thermal decomposition of SO_4^{2-} forming small molecular gases via high temperature treatment [43] make carbon nanosheets achieve higher MSA and MPV, which is verified in Fig. 4b. Herein, $CoSO_4$ served as additional molten salt can effectively tailor the MSA and MPV during the carbonization processes.

The structural characteristics of all samples were also carried out to ascertain the defected structure by Raman spectra. Fig. 5 depicts that Fe-N-Cs, Fe/Co-N-Cs and Fe/Co-N/S-Cs all exhibit characteristic D band at about 1335 cm^{-1} and G band at 1592 cm^{-1}. D band is related to disordered/defected carbon while G band ascribes to graphitic carbon structures. Therefore, the intensity ratio of band (I_D/I_G) commonly acts as revealing the defected structure of carbon. The I_D/I_G value of Fe-N-Cs, Fe/Co-N-Cs and Fe/Co-N/S-Cs is 2.858, 2.854, 3.027, respectively, indicating Fe/Co-N/S-Cs higher disordered/defected degree. The Co atom doping does not change the graphitic or defected structures of carbon, whereas more defected structures can be induced by doping S heteroatom, which is consistent with reported literature [44]. What's more, the carbon-based materials with relatively more defected structures can obviously accelerate the electrochemical reaction of ORR [16,45].

The atomic force microscopy (AFM) images (in Fig. 6) was also measured to evaluate the thickness of doped carbon nanosheets for Fe/Co-N/S-Cs. Fig. 6 implies that Fe/Co-N/S-Cs exhibits ultrathin nanosheet with thickness of 4.43 nm. Meanwhile, the thickness of the same nanosheetat at different locations was investigated in Fig. S6, indicating the nanosheet with thickness of 4.79 nm and 4.66 nm at different locations. Based on the analyses of AFM images, Fe/Co-N/S-Cs exhibits the ultrathin nanosheet with extremely uniform thickness, which can offer abundant catalytic active sites exposed to multiphase reaction interface for ORR and OER processes.

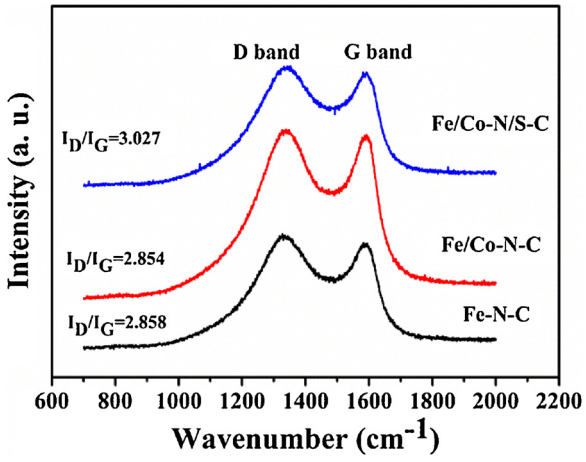

Fig. 5. Raman spectra of Fe-N-Cs, Fe/Co-N-Cs and Fe/Co-N/S-Cs.

3.2. Electrochemical properties of catalysts

The cyclic voltammetry (CV) technique was first adopted to estimate the catalytic performance of heteroatom-doped carbon nanosheets for ORR in potassium hydroxide aqueous solution (0.1 M) by rotating disk electrode (RDE). The CV profiles (in Fig. 7a) show that there are obvious reduction peaks for all samples in O_2-saturated environment but no obvious reduction peaks appear in N_2-saturated environment, indicating all samples present catalytic activity for ORR. The reduction peak potential of Fe/Co-N/S-Cs at 0.824 V vs RHE is higher than those of Fe/Co-N-Cs at 0.813 V and Fe-N-Cs at 0.795 V, respectively. Obviously, Fe/Co-N/S-Cs possesses more excellent electrocatalytic performance for ORR because more positive reduction peak potential represents higher ORR activity.

To further compare the ORR activity of all samples, the LSV tests were also carried out at rotation speed of 1600 rpm in O_2-saturated KOH solution. The half-wave potential ($E_{1/2}$) and limiting current density (I_{ld}) of Fe/Co-N/S-Cs obtained from LSV curves (in Fig. 7b) are 0.835 V and 6.77 mA cm^{-2}, which surpass the parameters of Fe/Co-N-Cs ($E_{1/2}$ = 0.832 V, I_{ld} = 5.67 mA cm^{-2}) and Fe-N-Cs ($E_{1/2}$ = 0.813 V, I_{ld} = 5.79 mA cm^{-2}). To further prove ORR active sites of Fe/Co-N/S-Cs, the poison experiments with 10 mM NaSCN are carried out because SCN- can poison Fe-Nx /Co-Nx sites. The experimental results (in Fig. S7) show that $E_{1/2}$ and I_{ld} of Fe/Co-N/S-Cs both decrease slightly after adding NaSCN. Based on the ORR polarization curves and NaSCN poison experiments, the excellent ORR activity can be mainly attributed to an appropriate amount of carbon defects tailored by doping thiophene sulfur [12,14–16,45], while bimetallic (Fe/Co) dopants with coexistence of active Fe-Nx/Co-Nx sites [10,11,38] partially improve ORR activity of carbonous materials. Compared to commercial Pt/C ($E_{1/2}$ = 0.839 V, I_{ld} = 5.80 mA cm^{-2}), Fe/Co-N/S-Cs exhibit close $E_{1/2}$ and higher I_{ld}. Hence, the Fe/Co-N/S-Cs synthesized by mixing molten salt-template ($FeCl_3$ and $CoSO_4$) exhibit prominent ORR activity.

Furthermore, the LSV curves were determined to probe the kinetic parameters of ORR process at various rotation rates (from 2000 to 400 rpm, in Fig. S8) on the basis of Koutechy–Levich (K–L) equation (detailed explanation in supplementary information). As shown in Fig. 7c, the calculated electron transfer number (n) for Fe-N-Cs, Fe/Co-N-Cs and Fe/Co-N/S-Cs is 3.22, 3.33 and 3.96, respectively, indicating a 2 e^- and 4 e^- ORR process for Fe-N-Cs and Fe/Co-N-Cs and preferable 4 e- ORR process for Fe/Co-N/S-Cs. These results imply that Fe/Co-N/S-

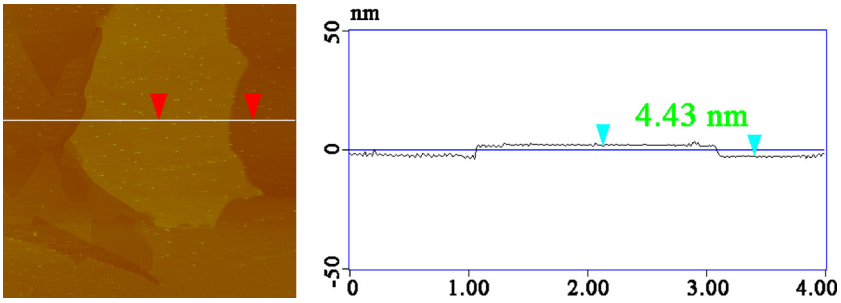

Fig. 6. AFM image and corresponding thickness profiles of Fe/Co-N/S-Cs.

Cs possess high catalytic selectivity for reducing O_2 to H_2O rather than to H_2O_2 [46,47]. Furthermore, rotating ring-disk electrode (RRDE) measurements show that the electron transfer number (n) is between 3.96 and 3.93, agreeing with calculated value from the K–L equations and H_2O_2 yield is below 3.5% in the voltage range from 0.3 V to 0.8 V, verifying a desired four-electron ORR process for Fe/Co-N/S-Cs (in Fig. S9).

For commercial application of rechargeable zinc-air batteries, it is extremely vital to design bifunctional electrocatalysts (ORR and OER activity). Therefore, the OER activity of three samples and Pt/C by LSV was measured in alkaline medium at 1600 rpm. As shown in Fig. 7d, the potential at 10 mA cm^{-2} ($E_{i=10}$) of Fe-N-Cs, Fe/Co-N-Cs, Fe/Co-N/S-Cs, Pt/C and RuO_2 is 1.558, 1.522, 1.515, 1.912 V and 1.573 V, respectively, and OER catalytic activity of Fe/Co-N/S-Cs is superior to that of RuO_2. Based on these analyses, Co dopant greatly improves OER activity of carbonous materials. To further prove OER active sites of Fe/Co-N/S-Cs, the poison experiments with 10 mM NaSCN are also carried out. The experimental results (in Fig. S10) show that $E_{i=10}$ of Fe/Co-N/S-Cs gives rise to a 96 mV positive shift after adding NaSCN, indicating that active Fe-Nx/Co-Nx sites [10,11] play an important role in enhancing OER activity of carbonous materials. The Fe/Co-N/S-Cs with lowest value of $E_{i=10}$ exhibit extremely superior OER catalytic activity compared to Fe-N-Cs, Fe/Co-N-Cs and Pt/C. Moreover, the △E ($\Delta E = E_{i=10} - E_{1/2}$) serves as a metric to evaluate bifunctional Electrocatalytic properties. Based on Fig. 7b and d, the △E of Fe-N-Cs, Fe/Co-N-Cs, Fe/Co-N/S-Cs and Pt/C is 0.745, 0.690, 0.680 and 1.073 V, respectively. The △E reported by other researchers is summarized in Table S4 and Fe/Co-N/S-Cs show smaller △E value than most of reported investigations, indicating that Fe/Co-N/S-Cs possess impressively excellent bifunctional electrocatalysts. Furthermore, the Fe/Co-N/S-Cs display less charge transfer resistance than that of Fe-N-Cs and Fe/Co-N-Cs by the EIS in Fig. S11.

Simultaneously, chronoamperometry measurements were also performed to assess the resistance to methanol and stability of Fe/Co-N/S-Cs at 1600 rpm. As shown in Fig. 8a, as soon as 3 M CH_3OH was added into electrolyte at about 400 s, an abrupt decrease of current for Pt/C electrode was immediately observed whereas the change of current for Fe/Co-N/S-Cs electrode was negligible, revealing that Fe/Co-N/S-Cs catalysts still maintain high catalytic activity in electrolyte solution with CH_3OH. Besides, the current-time curves (in Figs. 8b and S12) show that Fe/Co-N/S-Cs catalysts can maintain relatively high current density after continuous operation for 10 h, clearly exhibiting

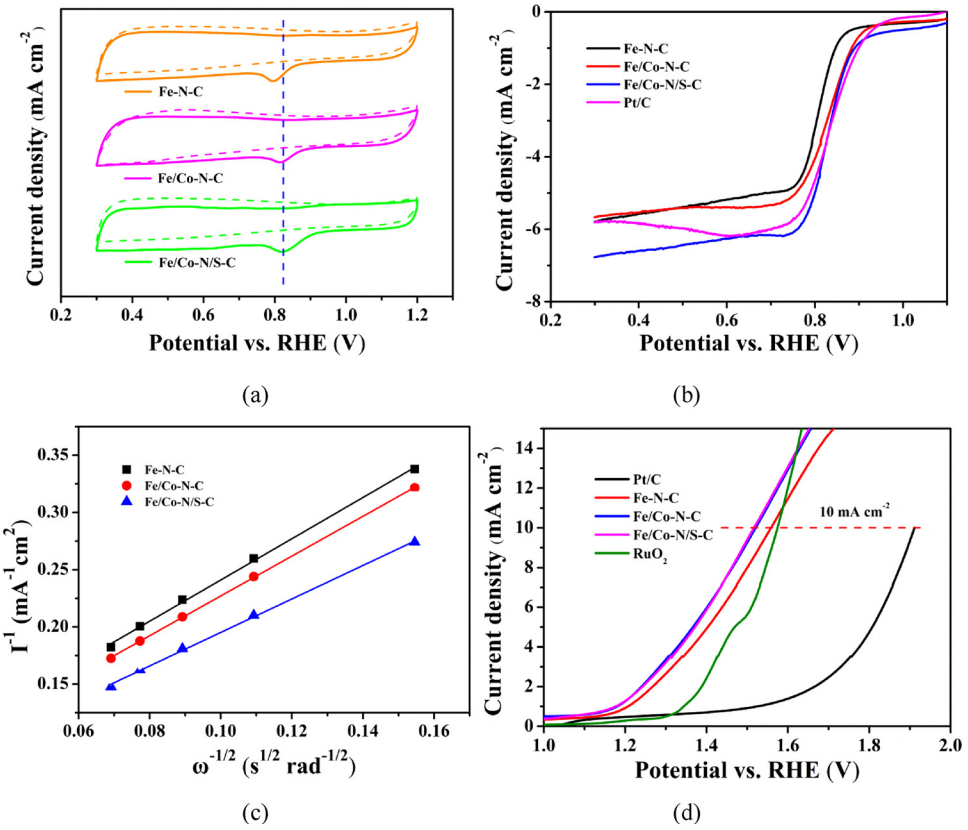

Fig. 7. (a) CV profiles of Fe-N-Cs, Fe/Co-N-Cs and Fe/Co-N/S-Cs in O_2- (solid) and N_2- saturated (dotted) KOH media ; (b) ORR curves of Fe-N-Cs, Fe/Co-N-Cs, Fe/Co-N/S-Cs and Pt/C; (c) Koutecky–Levich plots of Fe-N-Cs, Fe/Co-N-Cs, Fe/Co-N/S-Cs at 0.7 V according to Fig. S4; (d) OER curves of Fe-N-Cs, Fe/Co-N-Cs, Fe/Co-N/S-Cs, Pt/C and RuO_2.

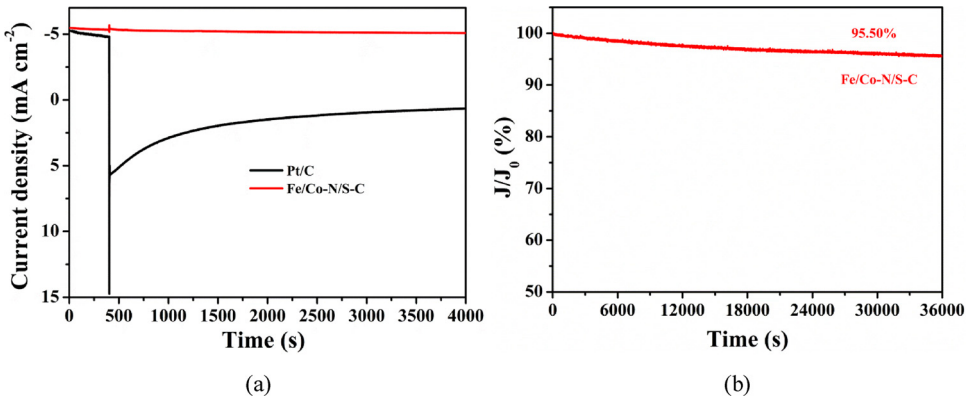

Fig. 8. (a) Chronoamperometric response of Fe/Co-N/S-Cs and Pt/C for ORR with CH_3OH after about 400 s at 0.75 V; (b) current-time curve of Fe/Co-N/S-Cs for 10 h at 0.75 V. The rotation rate is fixed at 1600 rpm.

remarkable ORR and OER durability.

3.3. Zn-air battery measures

On account of Fe/Co-N/S-Cs as excellent bifunctional electrocatalysts (in Fig. 9a), the self-made zinc-air batteries were assembled by zinc foil as negative electrode, carbon paper including catalysts (1.0 mg cm^{-2}) as positive electrode to evaluate practical application of as-synthesized catalysts. As shown in Fig. 9b, the zinc-air batteries with Fe/Co-N/S-Cs catalysts exhibit relatively stable an open circuit voltage of 1.395 V, which is negligibly low to that of Pt/C-based zinc-air batteries (1.410 V). Furthermore, as shown in Fig. 9c, Fe/Co-N/S-Cs-based Zn-air batteries exhibit higher discharging voltage (e.g., 1.051 V at 50 mA cm^{-2}) than that of Pt/C (e.g., 1.044 V at 50 mA cm^{-2}). Besides, Fe/Co-N/S-Cs-based zinc-air batteries show higher peak power density of 102.63 mW cm^{-2} at 0.669 V, while Pt/C-based zinc-air batteries exhibit low peak power density of 92.01 mW cm^{-2} at 0.636 V. This trend well agrees with the ORR polarization curves shown in Fig. 7b, where Fe/Co-N/S-Cs exhibit close $E_{1/2}$ and higher I_{ld} compared to commercial Pt/C. The discharge-charge measure was performed to evaluate the stability of Fe/Co-N/S-Cs catalyst for rechargeable Zn-air batteries (in Fig. 9d). The battery exhibits low initial voltage gap of 0.62 V between charge voltage (1.86 V) and discharge voltage (1.24 V) with round-trip efficiency of 66.67%. After 80 cycles (1600 min), the

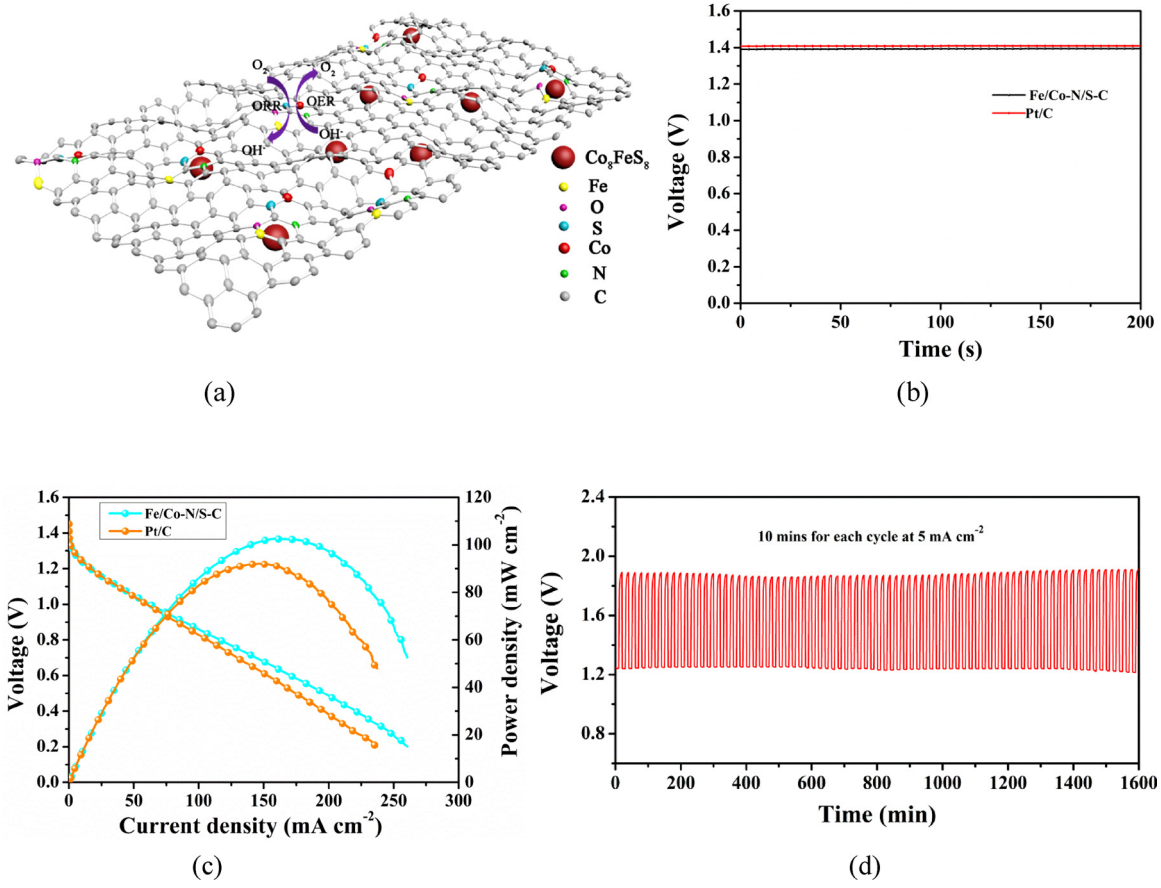

Fig. 9. (a) The Schematic illustration of Fe/Co-N/S-Cs as excellent bifunctional electrocatalysts; (b) open circuit curves of zinc-air batteries with Fe/Co-N/S-Cs and Pt/C catalysts; (c) polarization and power density profiles of Zn-air batteries with cathodic catalyst loaded by Fe/Co-N/S-Cs and Pt/C at 10 mV s^{-1}; (d) cyclic stability of Fe/Co-N/S-Cs-based Zn-air batteries at 5 mA cm^{-2}.

voltage gap only increases to 0.69 V with round-trip efficiency of 63.68%, further confirming that excellent stability and bifunctional electrocatalysis of Fe/Co-N/S-Cs can make rechargeable Zn-air batteries run stable for long time. Furthermore, SEM and TEM images of Fe/Co-N/S-Cs exhibit that the layered structure of Fe/Co-N/S-Cs does not obviously change after 40 and 80 circles of discharge-charge processes (in Fig. S13). To sum up, the remarkable bifunctional performance of Fe/Co-N/S-Cs for ORR and OER can be attributed to following factors: (i) 2D ultrathin porous carbon nanosheets can provide superior electrical charge transfer pathways; (ii) Fe/Co-N/S-Cs exhibit ultrahigh specific surface area and total pore volume; (iii) Uniformly distributed heteroatom dopants can expose more active sites; (iv) intrinsic carbon defects can be effectively tailored by doping thiophene sulfur.

4. Conclusions

In conclusion, we have developed a control-easy, environmentally-friendly and scalable synthesis route to achieve 2D layered Fe/Co and N/S codoping porous carbon nanosheets (Fe/Co-N/S-Cs) by a novel and multifunctional inorganic mixing salt-template. Fe/Co-N/S-Cs with uniform and ultrathin thickness of about 4.63 nm exhibit ultrahigh SSA ($1589\ m^2\ g^{-1}$) and TPV ($0.92\ cm^3\ g^{-1}$), homogeneous distribution of heteroatom dopants, as well as an appropriate amount of carbon defects. Co dopant greatly improves OER activity, while S dopant mainly enhances ORR activity compared to Fe-N-Cs. The resultant Fe/Co-N/S-Cs display effectively bifunctional performance for ORR and OER with ultralow ΔE ($\Delta E = E_{i=10} - E_{1/2}$) of 0.68 V in alkaline solution. Furthermore, the assembled Zn-air batteries employing Fe/Co-N/S-Cs as cathode catalyst exhibit high OCP of 1.395 V, power density ($102.63\ mW\ cm^{-2}$) and excellent stability. The novel inorganic salt mixing template offers a facile, environmental-friendly and scalable preparation route to rationally design practical and high-active 2D heteroatom-doped hierarchical porous carbon nanosheets, which sheds light on fabrication of superior but cheap electrocatalysts for developing next energy-related storage technology.

Acknowledgments

This study was fundedby National Natural Science Foundation of China (Grant Numbers 51372191, 51102189), National Basic Research Program of China (Grant Number 2015CB656401). The authors declare that they have no conflict of interest.

Appendix A. Supplementary data

Supplementary material related to this article can be found, in the online version, at doi:https://doi.org/10.1016/j.apcatb.2018.09.024.

References

[1] R. Raccichini, A. Varzi, S. Passerini, B. Scrosati, The role of graphene for electrochemical energy storage, Nat. Mater. 14 (2015) 271–279.
[2] J. Yin, Y. Li, F. Lv, M. Lu, K. Sun, W. Wang, L. Wang, F. Cheng, Y. Li, P. Xi, S. Guo, Oxygen vacancies dominated NiS_2/CoS_2 interface porous nanowires for portable Zn-air batteries driven water splitting devices, Adv. Mater. 29 (2017) 1704681.
[3] H. Tang, Y. Zeng, Y. Zeng, R. Wang, S. Cai, C. Liao, H. Cai, X. Lu, P. Tsiakaras, Iron embedded nitrogen doped carbon frameworks as robust catalyst for oxygen reduction reaction in microbial fuel cells, Appl. Catal. B: Environ. 202 (2017) 550–556.
[4] J. Wu, H. Yang, Platinum-based oxygen reduction electrocatalysts, Acc. Chem. Res. 46 (2013) 1848–1857.
[5] W. Li, Y. Xiong, Z. Wang, M. Bao, J. Liu, D. He, S. Mu, Seed-mediated synthesis of large-diameter ternary TePtCo nanotubes for enhanced oxygen reduction reaction, Appl. Catal. B: Environ. 231 (2018) 277–282.
[6] H. Lv, X. Chen, D. Xu, Y. Hua, H. Zheng, S.L. Sui, Ben Liu, Ultrathin PdPt bimetallic nanowires with enhanced electrocatalytic performance for hydrogen evolution reaction, Appl. Catal. B: Environ. 238 (2018) 525–532.
[7] K. Wan, G.-F. Long, M.-Y. Liu, L. Du, Z.-X. Liang, P. Tsiakaras, Nitrogen-doped ordered mesoporous carbon: synthesis and active sites for electrocatalysis of oxygen reduction reaction, Appl. Catal. B: Environ. 165 (2015) 566–571.
[8] D. Deng, L. Yu, X. Chen, G. Wang, L. Jin, X. Pan, J. Deng, G. Sun, X. Bao, Iron encapsulated within pod-like carbon nanotubes for oxygen reduction reaction, Angew. Chem. Int. Ed. 52 (2013) 371–375.
[9] S. Cai, Z. Meng, H. Tang, Y. Wang, P. Tsiakarasc, 3D Co-N-doped hollow carbon spheres as excellent bifunctionalelectrocatalysts for oxygen reduction reaction and oxygen evolutionreaction, Appl. Catal. B: Environ. 217 (2017) 477–484.
[10] Q. Lin, X. Bu, A. Kong, C. Mao, F. Bu, P. Feng, Heterometal-embedded organic conjugate frameworks from alternating monomeric Iron and cobalt metalloporphyrins and their application in design of porous carbon catalysts, Adv. Mater. 27 (2015) 3431–3436.
[11] Z. Zhang, M. Dou, H. Liu, L. Dai, F. Wang, A facile route to bimetal and nitrogen-codoped 3D porous graphitic carbon networks for efficient oxygen reduction, Small 12 (2016) 4193–4199.
[12] D.-H. Kwak, S.-B. Han, D.-H. Kim, J.-E. Won, K.-W. Park, Amino acid-derived non-precious catalysts with excellent electrocatalytic performance and methanol tolerance in oxygen reduction reaction, Appl. Catal. B: Environ. 238 (2018) 93–103.
[13] Y.Y. Guo, P.F. Yuan, J.N. Zhang, Y.F. Hu, I.S. Amiinu, X. Wang, J.G. Zhou, H.C. Xia, Z.B. Song, Q. Xu, S.C. Mu, Carbon nanosheets containing discrete Co-Nx-By-C active sites for efficient oxygen electrocatalysis and rechargeable Zn-air batteries, ACS Nano 12 (2018) 1894–1901.
[14] K.G. Qu, Y. Zheng, Y. Jiao, X.X. Zhang, S. Dai, S.Z. Qiao, Polydopamine-inspired dual heteroatom-doped carbon nanotubes for highly efficient overall water splitting, Adv. Funct. Mater. 7 (2017) 1602068.
[15] K. Qu, Y. Zheng, S. Dai, S.Z. Qiao, Graphene oxide-polydopamine derived N, S-codoped carbon nanosheets as superior bifunctional electrocatalysts for oxygen reduction and evolution, Nano Energy 19 (2016) 373–381.
[16] J. Zhu, W. Li, S. Li, J. Zhang, H. Zhou, C. Zhang, J. Zhang, S. Mu, Defective N/S-codoped 3D cheese-like porous carbon nanomaterial toward efficient oxygen reduction and Zn-air batteries, Small 14 (2018) 1800563.
[17] J. Yang, X. Wang, B. Li, L. Ma, L. Shi, Y. Xiong, H. Xu, Novel iron/cobalt-containing polypyrrole hydrogel-derived trifunctional electrocatalyst for self-powered overall water splitting, Adv. Funct. Mater. 27 (2017) 1606497.
[18] M.-Q. Wang, C. Ye, M. Wang, T.-H. Li, Y.-N. Yu, S.-J. Bao, Synthesis of M (Fe_3C, Co, Ni)-porous carbon frameworks as high-efficient ORR catalysts, Energy Storage Mater. 11 (2018) 112–117.
[19] C.Y. Su, H. Cheng, W. Li, Z.Q. Liu, N. Li, Z. Hou, F.Q. Bai, H.X. Zhang, T.Y. Ma, Atomic modulation of FeCo-nitrogen-carbon bifunctional oxygen electrodes for rechargeable and flexible all-solid-state zinc-air battery, Adv. Energy Mater. 7 (2017) 1602420.
[20] N. Fechler, T.-P. Fellinger, M. Antonietti, “Salt templating”: a simple and sustainable pathway toward highly porous functional carbons from ionic liquids, Adv. Mater. 25 (2013) 75–79.
[21] C. Wang, D. Wu, H. Wang, Z. Gao, F. Xua, K. Jiang, A green and scalable route to yield porous carbon sheets from biomass for supercapacitors with high capacity, J. Mater. Chem. A 6 (2018) 1244–1254.
[22] C. Nita, M. Bensafia, C. Vaulot, L. Delmotte, C.M. Ghimbeu, Insights on the synthesis mechanism of green phenolic resin derived porous carbons via a salt-soft templating approach, Carbon 109 (2016) 227–238.
[23] T. Ouyang, K. Cheng, Y. Gao, S. Kong, K. Ye, G. Wang, D. Cao, Molten salt synthesis of nitrogen doped porous carbon: a new preparation methodology for high-volumetric capacitance electrode materials, J. Mater. Chem. A 4 (2016) 9832–9843.
[24] Y.-B. Huang, P. Pachfule, J.-K. Sun, Q. Xu, From covalent-organic frameworks to hierarchically porous B-doped carbons: a molten-salt approach, J. Mater. Chem. A 4 (2016) 4273–4279.
[25] K. Yuan, X. Zhuang, H. Fu, G. Brunklaus, M. Forster, Y. Chen, X. Feng, U. Scherf, Two-dimensional core-shelled porous hybrids as highly efficient catalysts for the oxygen reduction reaction, Angew. Chem. Int. Ed. 55 (2016) 6858–6863.
[26] S. Liu, P. Gordiichuk, Z.-S. Wu, Z. Liu, W. Wei, M. Wagner, N. Mohamed-Noriega, D. Wu, Y. Mai, A. Herrmann, K. Müllen, X. Feng, Patterning two-dimensional free-standing surfaces with mesoporous conducting polymers, Nat. Commun. 6 (2015) 8817.
[27] M.A. Squillaci, F. Qiu, A. Aliprandi, F. Zhang, X. Feng, P. Samorì, Direct patterning of organic functional polymers through conventional photolithography and non-invasive cross-link agents, Adv. Mater. 28 (2016) 5249–5254.
[28] L. Wang, Y. Zhu, C. Guo, X. Zhu, J. Liang, Y. Qian, Ferric chloride-graphite intercalation compounds as anode materials for Li-ion batteries, ChemSusChem 7 (2014) 87–91.
[29] Q. Wei, F. Zhang, J. Li, B. Li, C. Zhao, Oxidant-induced dopamine polymerization for multifunctional coatings, Polym. Chem. 1 (2010) 1430–1433.
[30] M. Li, H. Zhou, W. Yang, L. Chen, Z. Huang, N. Zhang, C. Fu, Y. Kuang, Co_9S_8 nanoparticles embedded in a N, S co-doped graphene-unzipped carbon nanotube composite as a high performance electrocatalyst for the hydrogen evolution reaction, J. Mater. Chem. A 5 (2017) 1014–1021.
[31] D. Xiong, Q. Zhang, S.M. Thalluri, J. Xu, W. Li, X. Fu, L. Liu, One-step fabrication of monolithic electrodes comprising Co9S8 particles supported on cobalt foam for efficient and durable oxygen evolution reaction, Chem. Eur. J. 23 (2017) 8749–8755.
[32] S. Liu, M. Tong, G. Liu, X. Zhang, Z. Wang, G. Wang, W. Cai, H. Zhang, H. Zhao, S, N-containing Co-MOF derived Co_9S_8@ S, N-doped carbon materials as efficient oxygen electrocatalysts and supercapacitor electrode, Mater. Chem. Front. 4 (2017) 491–498.
[33] T. Vargaa, G. Ballaia, L. Vásárhelyia, H. Haspela, Á. Kukovecza, Z. Kónyaa, Co4N/nitrogen-doped graphene: a non-noble metal oxygen reduction electrocatalyst for alkaline fuel cells, Appl. Catal. B: Environ. 237 (2018) 826–834.
[34] M. Shen, L.-R. Zheng, W. He, C. Ruan, C. Jiang, K. Ai, L. Lu, High-performance oxygen reduction electrocatalysts derived from uniform cobalt-adenine assemblies,

Nano Energy 17 (2015) 120–130.
[35] Y. Ding, Y. Niu, J. Yang, L. Ma, J. Liu, Y. Xiong, H. Xu, A metal-amino acid complex-derived bifunctional oxygen electrocatalyst for rechargeable zinc-air batteries, Small 12 (2016) 5414–5421.
[36] Q. Wei, X. Yang, G. Zhang, D. Wang, L. Zuin, D. Banham, L. Yang, S. Ye, Y. Wang, M. Mohamedi, S. Sun, An active and robust Si-Fe/N/C catalyst derived from waste reed for oxygen reduction, Appl. Catal. B: Environ. 237 (2018) 85–93.
[37] W. Yang, X. Liu, X. Yue, J. Jia, S. Guo, Bamboo-like carbon nanotube/Fe_3C nanoparticle hybrids and their highly efficient catalysis for oxygen reduction, J. Am. Chem. Soc. 137 (2015) 1436–1439.
[38] J. Yin, Y. Li, F. Lv, Q. Fan, Y.-Q. Zhao, Q. Zhang, W. Wang, F. Cheng, P. Xi, S. Guo, NiO/CoN porous nanowires as efficient bifunctional catalysts for Zn-air batteries, ACS Nano 11 (2017) 2275–2283.
[39] M.-H. Ryou, J. Kim, I. Lee, S. Kim, Y.K. Jeong, S. Hong, J.H. Ryu, T.-S. Kim, J.-K. Park, H. Lee, J.W. Choi, Mussel-inspired adhesive binders for high-performance silicon nanoparticle anodes in lithium-ion batteries, Adv. Mater. 25 (2013) 1571–1576.
[40] H. Jiang, L. Yang, C. Li, C. Yan, P.S. Lee, J. Ma, High-rate electrochemical capacitors from highly graphitic carbon-tipped manganese oxide/mesoporous carbon/manganese oxide hybrid nanowires, Energy Environ. Sci. 4 (2011) 1813–1819.
[41] M. d'Ischia, A. Napolitano, A. Pezzella, P. Meredith, T. Sarna, Chemical and structural diversity in eumelanins: unexplored bio-optoelectronic materials, Angew. Chem. Int. Ed. 48 (2009) 3914–3921.
[42] W. Wei, H. Liang, K. Parvez, X. Zhuang, X. Feng, K. Mgllen, Nitrogen-doped carbon nanosheets with size-defined mesopores as highly efficient metal-free catalyst for the oxygen reduction reaction, Angew. Chem. Int. Ed. 126 (2014) 1596–1600.
[43] M. Wu, J. Qiao, K. Li, X. Zhou, Y. Liu, J. Zhang, A large-scale synthesis of heteroatom (N and S) co-doped hierarchically porous carbon (HPC) derived from polyquaternium for superior oxygen reduction reactivity, Green Chem. 18 (2016) 2699–2709.
[44] X. Liu, M. Antonietti, Moderating black powder chemistry for the synthesis of doped and highly porous graphene nanoplatelets and their use in electrocatalysis, Adv. Mater. 25 (2013) 6284–6290.
[45] Jian Zhang, Chenyu Zhang, Yufeng Zhao, Ibrahim Saana Amiinu, Huang Zhou, Xiaobo Liu, Yongfu Tang, Shichun Mu, Three dimensional few-layer porous carbon nanosheets towardsoxygen reduction, Appl. Catal. B: Environ. 211 (2017) 148–156.
[46] T. Ikeda, M. Boero, S.-F. Huang, K. Terakura, M. Oshima, J.-I. Ozaki, Carbon alloy catalysts: active sites for oxygen reduction reaction, J. Phys. Chem. C 112 (2008) 14706–14709.
[47] H.W. Liang, X. Zhuang, S. Bruller, X. Feng, K. Mullen, Hierarchically porous carbons with optimized nitrogen doping as highly active electrocatalysts for oxygen reduction, Nat. Commun. 5 (2014) 4973.